PHYSICAL REVIEW E

STATISTICAL PHYSICS, PLASMAS, FLUIDS, AND RELATED INTERDISCIPLINARY TOPICS

THIRD SERIES, VOLUME 57, NUMBER 4 APRIL 1998

RAPID COMMUNICATIONS

The Rapid Communications section is intended for the accelerated publication of important new results. Since manuscripts submitted to this section are given priority treatment both in the editorial office and in production, authors should explain in their submittal letter why the work justifies this special handling. A Rapid Communication should be no longer than 4 printed pages and must be accompanied by an abstract. Page proofs are sent to authors.

Nonlinear dynamics at a Hopf bifurcation with axisymmetry breaking in a jet

Ionut Danaila,[1,2] Jan Dušek,[3] and Fabien Anselmet[2]
[1]*INERIS, Parc Tech. Alata, 60550 Verneuil en Halatte, France*
[2]*IRPHE, 12, Avenue Général Leclerc, 13003 Marseille, France*
[3]*IMF, 2 rue Boussingault, 67000 Strasbourg, France*
(Received 12 May 1997)

A complex dynamics with several bifurcations within a 4% variation of the Reynolds number has been found to accompany the transition from a steady to a chaotic flow in a homogeneous round fluid jet. The results of direct numerical simulations are explained using a fifth order weakly nonlinear theory describing the interaction of two counter-rotating helical modes, arising as a consequence of degeneracy of the linearized Navier-Stokes operator spectrum. Two secondary bifurcations and three different asymptotic states are shown to be correctly accounted for by the theory. The validity of the fifth order theory ceases shortly before the onset of chaos. [S1063-651X(98)50404-7]

PACS number(s): 05.45.+b, 47.20.Ft, 47.27.Wg, 47.27.Cn

During the transition to turbulence the existing symmetries are broken, which leads not only to more and more complicated spatial patterns [1] but also to an increasingly complex dynamics [2]. Many laminar flows, such as round jets and wakes of symmetric objects, are axisymmetric with respect to the flow direction. In wakes of a sphere and of a disc axisymmetry breaking has been shown to occur before the onset of instationarity [3,4]. In jets, the linear theory allowed to predict very early the pertinence of symmetry breaking helical modes for the primary instability [5]. At small Reynolds numbers the helical modes with azimuthal wave number $m=\pm 1$ are the most amplified, at higher Reynolds numbers the symmetry is conserved and the ''varicose'' $m=0$ mode is the most unstable [6,7]. The theory predicts, and all experimental and numerical investigations of round jets confirm, that the primary instability is accompanied by an onset of oscillations at a well defined frequency, i.e., the primary bifurcation is always of Hopf type in jets.

The theoretical work concerning the axisymmetry breaking in jets and wakes is mostly limited to the linear theory. However, nonlinear effects are of basic importance in determining the final state (attractor) of the instability. Recently, we undertook direct numerical simulations of a round jet in a chaotic regime close to its onset [8]. We focused mainly on coherent structures appearing at the onset chaos and persisting in turbulent jets. We noticed that Hopf-type oscillations and the well known helical modes $m=\pm 1$ characterize the linear regime in a rather wide interval of Reynolds numbers and that, for small Reynolds number variations, the final attractor varies considerably.

To explain this extreme sensitivity of the attractor to the Reynolds number, we investigated the instability onset. The common feature of experimental jets and of our simulation is that the dynamics is controlled by a single parameter: the flow-rate, quantified by the Reynolds number (Re), based on the maximum inflow velocity (U) and the nozzle diameter (D). The absolute value of the critical Reynolds number has no universal meaning by itself because cold jets can be considered rather as noise amplifiers [9] due to the convective nature of their instability [10]. In experiments, the noise generation in the nozzle is poorly controlled and varies from one experimental setup to another [9]. In numerical simulations, the instability onset depends on the numerical discretization close to the inflow. The critical Reynolds number lies between 220 and 320, depending on the numerical discretization and the numerical inflow velocity profile in our simulation. For the mentioned reasons we shall rather refer to the

instability parameter $\epsilon=(\mathrm{Re}-\mathrm{Re}_{crit})/\mathrm{Re}_{crit}$, with Re_{crit} the critical Reynolds number.

Let us assume a steady axisymmetric basic flow. In cylindrical coordinates with (z,r,θ) denoting the streamwise, radial, and azimuthal directions, it is characterized by the velocity $\mathbf{V}=(V_z,V_r,V_\theta=0)$ and pressure P fields independent of θ. The linear eigenvalue problem

$$\lambda\Phi+\mathcal{L}[\mathbf{V}]\Phi+\nabla\Pi=0;\quad \nabla\Phi=0 \tag{1}$$

is obtained by inserting a perturbed flow-field $\mathbf{v}=\mathbf{V}+e^{\lambda t}\mathbf{\Phi}+e^{\bar{\lambda}t}\bar{\mathbf{\Phi}}$, $p=P+e^{\lambda t}\Pi+e^{\bar{\lambda}t}\bar{\Pi}$ into nondimensionalized incompressible Navier-Stokes equations. Assuming the bifurcation to be of Hopf type, λ is complex and $(\bar{\lambda},\bar{\mathbf{\Phi}})$ is also solution of the eigenvalue problem (1). The linear operator $\mathcal{L}[\mathbf{V}]$ commutes with the derivative $\partial/\partial\theta$, which explains why common eigenfunctions of $\mathcal{L}[\mathbf{V}]$ and $\partial/\partial\theta$ can be sought. Let us write an element of the eigen-subspace of $\partial/\partial\theta$ associated with the eigenvalue $-im$ (m arbitrary integer) as: $\mathbf{\Phi}_m(r,\theta,z)\equiv\boldsymbol{\phi}_m(r,z)e^{-im\theta}$.

It is easily seen that $\mathcal{L}[\mathbf{V}]$ restricted to such an eigenspace has eigenvalues independent of the sign of m (see also [5]). Otherwise stated, each eigenspace $m\neq0$ is degenerate with two linearly independent eigenvectors $\mathbf{\Phi}_m$ and $\mathbf{\Phi}_{-m}$. Let $M>0$ be the value of m characterizing the most unstable eigensubspace $\mathrm{Real}\lambda_{m^2}\leqslant\mathrm{Real}\lambda_{M^2}$ and write $\lambda_{M^2}=\gamma_{M^2}+i\omega_{M^2}$ with ω_{M^2} chosen positive. Then an arbitrary element of the eigensubspace associated with λ_{M^2} can be written as an arbitrary complex linear combination of $\mathbf{\Phi}_M$ and $\mathbf{\Phi}_{-M}$. The asymptotic plane wave form $\mathbf{\Phi}_\pm\sim e^{-i(kz\pm M\theta)}$ gives the helical appearance of the unstable modes [8]. [Due to the fact that the pressure field can be eliminated and plays an auxiliary role in Navier-Stokes equations and in Eq. (1) we can characterize the eigenspace only by the perturbation of the velocity vector components]. In what follows, we assume $M=1$, and drop the M or M^2 subscripts.

When the unstable eigenvalue is non-degenerate, it has been shown [11] that the Landau model results as a third order weakly non-linear approximation of the full Navier-Stokes equations. The analysis of results of simulation of a nearly critical jet showed, however, that very early (at $\epsilon\sim0.02$) nonlinear effects of order higher than 3 are important for the instability saturation. The most straightforward way to introduce higher order weakly nonlinear theory is to follow the idea of Herbert [12] and assume the perturbation to be expandable into a power series of the projection of the fundamental onto the linear eigenmode.

The perturbation $e^{\lambda t}\Phi$ of the velocity field can be written as

$$e^{\lambda t}\Phi=[A_+(t)\phi_+e^{-i\theta}+A_-(t)\phi_-e^{i\theta}]e^{i\omega t}, \tag{2}$$

the exponential growth factor $e^{\gamma t}$ being included into $A_\pm$. As the linear mode grows, it generates higher order nonlinear terms and higher order harmonics [11]. The onset of higher order harmonics results in a Fourier series in θ, with a fundamental period of 2π. As far as the time dependence is concerned, the oscillations are not strictly periodic in the linear and transient regime due to the instability amplification and they do not have exactly the linear angular frequency ω at the instability saturation, due to the nonlinear frequency shift. These effects can be separated from the periodic time-behavior by introducing a separate time variable s, representing the perturbation $\mathbf{v}'=\mathbf{v}-\mathbf{V}$ as $\mathbf{v}'(r,\theta,z;t)=\tilde{\mathbf{v}}'(r,\theta,z;t,s)|_{s=t}$. The perturbation can now be assumed strictly periodic with period $2\pi/\omega$ as a function of t and expanded into a double Fourier series,

$$\tilde{\mathbf{v}}'(r,\theta,z;t,s)=\sum_{n,\ell=-\infty}^{\infty}\mathbf{c}_{n,\ell}(r,z;s)e^{in\omega t}e^{-i\ell\theta}, \tag{3}$$

where $\mathbf{c}_{n,\ell}(.,s)=\overline{\mathbf{c}_{-n,-\ell}(r,z;s)}$ are complex vectorial functions. A similar expansion, with scalar coefficients $d_{n,\ell}(r,z;s)$, can be written for the pressure field perturbation $\tilde{p}'(r,\theta,z;t,s)$. The Navier-Stokes equations yield then, in the same way as for a simple time Fourier expansion [11], a coupled system of equations

$$\begin{aligned}&\frac{\partial\mathbf{c}_{n,\ell}}{\partial s}e^{-i\ell\theta}+(in\omega+\mathcal{L}[\mathbf{V}])\mathbf{c}_{n,\ell}e^{-i\ell\theta}+\nabla(d_{n,\ell}e^{-i\ell\theta})\\&\quad+e^{-i\ell\theta}\sum_{k,j=-\infty}^{\infty}\mathbf{c}_{n-k,\ell-j}e^{ij\theta}\cdot\nabla(\mathbf{c}_{k,j}e^{-ij\theta})=0,\\&\nabla\cdot\mathbf{c}_{n,\ell}e^{-i\ell\theta}=0.\end{aligned} \tag{4}$$

As the instability grows, the nonlinear effects deviate the fundamental of oscillations from the unstable eigenspace. Therefore, strictly speaking, only the projections of $c_{1,\pm1}$ onto $\Phi_\pm$ can be written as $A_\pm(t)\phi_\pm$. Let us define the following scalar complex function ($\mathcal{P}_\pm$ standing for projection onto $\phi_\pm$) by

$$\mathcal{P}_\pm(c_{1,\pm1})e^{in\omega t\mp i\theta}=B_\pm(s,t,\theta)\phi_\pm, \tag{5}$$

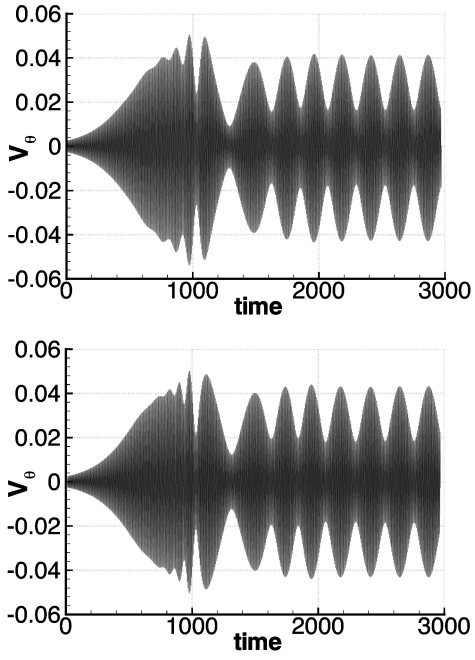

FIG. 1. Azimuthal velocity at a point situated at 2D downstream from the nozzle and at 0.5D off the flow axis of the flow at $(\mathrm{Re}-\mathrm{Re}_{crit})/\mathrm{Re}_{crit}=2\%$. The period of oscillations is about six time units. Simulated signal (top) and modeled signal (bottom) with the fifth order weakly nonlinear model.

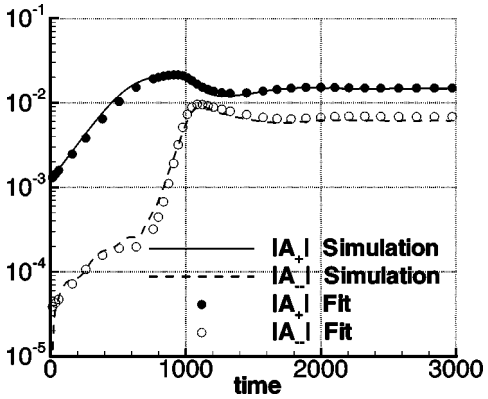

FIG. 2. Amplitudes of helical modes $n=1$, $\ell=\pm1$ and their fits as functions of time (the $\sim$ sign in $\tilde{A}_\pm$ is omitted).

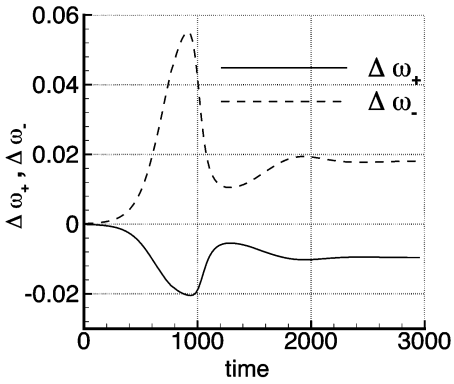

FIG. 3. Nonlinear angular velocity shifts of helical modes $n=1$, $\ell=\pm1$ and their fits as functions of time.

where $B_\pm \equiv A_\pm(s)e^{in\omega t \mp i\theta}$. In the linear regime, the perturbation is identical to the sum of projections $B_\pm\phi_\pm$ and their complex conjugates, with independent amplitudes $B_\pm$. When nonlinear effects set in, the perturbation can be considered [12] as an analytic function of B_+ and B_- with $B_\pm\phi_\pm$ as leading terms:

$$\tilde{\mathbf{v}}'(r,\theta,z;t,s)=\sum \beta_{j,k,p,q}B_+^j B_-^k \overline{B_+^p B_-^q}, \qquad (6)$$

with $j,k,p,q\geqslant 0$ and $j+k+p+q\geqslant 1$. A general term of the power series (6) contributes to a well defined harmonic of the Fourier expansion (3). Consequently, only terms of Eq. (6) for which $j+k-p-q=n$ and $j-k-p+q=\ell$ contribute to $c_{n,\ell}$. This implies that $n+\ell$ must be an even number and that

$$c_{n,\ell}=A_+{}^{|n+\ell|/2}A_-{}^{|n-\ell|/2}\sum_{j,k=0}^{\infty}\alpha_{k,j}^{(n,\ell)}|A_+|^{2k}|A_-|^{2j}, \quad (7)$$

with $\alpha_{k,j}^{(n,l)}(r,z)$ s-independent complex vector functions of space variables. In particular, by Eq. (5), $\alpha_{0,0}^{(1,\pm1)}\equiv\phi_\pm$. The power expansions (7) and Eqs. (4) allow to write finite truncated systems of arbitrary order of precision in $A_\pm$. Let us remark that the leading order of terms in the equation for $n=1$, $\ell=1$ is three in the same way as in the ordinary Landau model. For this reason, it is sufficient to account only for third order terms in the expansion of $c_{1,1}$: $c_{1,1}\approx A_+(\phi_+ +\alpha|A_+|^2+\beta|A_-|^2)$, where $\alpha\equiv\alpha_{1,0}^{(1,1)}$ and $\beta\equiv\alpha_{0,1}^{(1,1)}$. Using Eq. (1) and dropping terms of higher order than 5, we arrive at the following equation:

$$\frac{1}{A_+}\frac{d}{ds}[A_+(\phi_+ +\alpha|A_+|^2+\beta|A_-|^2)]$$
$$=\gamma\phi_+ -(\eta_+|A_+|^2+\eta_-|A_-|^2)$$
$$-(\eta_{+,+}|A_+|^4+\eta_{+,-}|A_+|^2|A_-|^2+\eta_{-,-}|A_-|^4). \qquad (8)$$

By symmetry, the same equation with $A_+\to A_-$ holds for $n=1$ and $\ell=-1$. Equation (8) can be interpreted as a generalized Landau model in various ways. It can either be projected onto ϕ_+ (Note that, by definition of $A_\pm$, $\mathcal{P}_\pm\alpha=\mathcal{P}_\pm\beta=0$.) or used to describe the evolution of the amplitude of oscillations of the fundamental at some given point in space [11]. The second point of view is easier to illustrate by numerical simulations or experimentally. In that case, we introduce, at a given point r_0,z_0 and for a given velocity component, say θ: $\tilde{A}_+(s)\equiv c_{1,1,\theta}(r_0,z_0;s)\approx A_+(\phi_{\theta,+}+\alpha_\theta|A_+|^2+\beta_\theta|A_-|^2)|_{r_0,z_0}$. For $A_+\to A_-$ we similarly define $\tilde{A}_-(s)$. Assuming $\phi_{\theta,\pm}(r_0,z_0)\neq 0$ and extracting $A_\pm$ as functions of $\tilde{A}_\pm$ to the third order of precision we arrive at the following system of two coupled equations:

$$\frac{1}{\tilde{A}_\pm}\frac{d}{ds}\tilde{A}_\pm=\gamma-(C|\tilde{A}_\pm|^2+D|\tilde{A}_\mp|^2$$
$$-(a|\tilde{A}_\pm|^4+b|\tilde{A}_\pm|^2|\tilde{A}_\mp|^2+c|\tilde{A}_\mp|^4), \qquad (9)$$

where C,D,a,b, and c are, by symmetry, the same complex, r_0 and z_0 depending, coefficients in both equations.

In a simulation of a low Reynolds number jet ($\mathrm{Re}=225$, $\mathrm{Re}_{crit}=220$, $\epsilon=0.023$) we set an initial condition with a practically pure perturbation proportional to the eigen-mode ϕ_+. It was obtained by adding the pure helical mode $ac_{1,1}$ + c.c. extracted from a previous simulation of the instability in the phase of development to the unperturbed steady axisymmetric flow at $t=0$. The reduction factor a is chosen to yield a perturbation amplitude of only 10^{-3} of the inflow velocity, so as to capture the linear regime. The behavior of the simulated signal of the azimuthal velocity v_θ at an arbitrarily chosen point off the flow axis is represented in Fig. 1 (top). It can easily be explained by the simplified model (9). Indeed, by fitting separately the real and imaginary parts of the coefficients in Eqs. (9), using the calculated values of the

TABLE I. Values of the amplification rate and of the linear Strouhal frequency and of the constants of the fifth order nonlinear model fitted to the signal in Fig. 1.

	$\gamma+i\omega$	C	D	a	b	c
Real	4.43×10^{-3}	8.2	54.6	1.15×10^{3}	3.55×10^{4}	-1.69×10^{5}
Im	1.068	56.8	−84.5	-2.75×10^{4}	2.25×10^{5}	-8.03×10^{4}

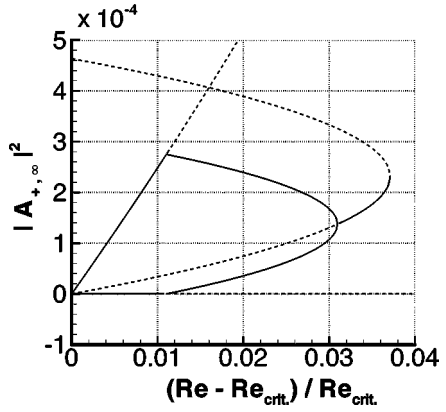

FIG. 4. Bifurcation diagram of asymptotic values of $|\tilde{A}_+|^2$ vs $(\mathrm{Re}-\mathrm{Re}_{crit})/\mathrm{Re}_{crit}$. Note the transcritical, inverse pitchfork and saddle node bifurcations.

azimuthal components of the modes ($c_{1,\pm 1,\theta}$) at this point, we obtain the modeled signal of Fig. 1 (bottom). The time evolution of the moduli $|\tilde{A}_\pm|$ is represented in Fig. 2, that of the nonlinear frequency shifts $\Delta\omega_\pm \equiv d\ \arg(\tilde{A}_\pm)/ds$ is plotted in Fig. 3. The linear amplification rate and Strouhal frequency together with the local values of constants C,D,a,b, and c are assembled in Table I.

The linear regime, with modes $n=1$, $\ell=\pm 1$ amplified exponentially with the same amplification rate, extends until approximately $t\approx 350\,D/U$ time units. (See Fig. 2.) At $t\approx 350$ the third order weakly nonlinear regime sets in. The amplification of the weaker mode ($\tilde{A}_-$) slows down and without higher order effects this mode would, ultimately, completely decay. At $t\approx 650$ the fifth order effects become perceptible. Between $t\approx 650$ and $t\approx 1100$ the mode $\ell=-1$ is strongly amplified via the last term on the right-hand side of the second Eq. (9), with c having a large negative real part (see Table I). The amplification of mode $\ell=-1$ results in a dampening of mode $\ell=1$ via the third order term containing the constant D. Ultimately, at about $t\approx 1900$ both amplitudes $|\tilde{A}_\pm|$ become steady and a saturation (asymptotic state) is reached. The asymptotic angular velocity shifts obtained from Eq. (9) are then different (see Fig. 3) causing the limit torus dynamics visible in Fig. 1.

The possible asymptotic states can easily be predicted assuming that very close to the threshold, say for $\epsilon \leqslant 0.05$, all parameters of the fifth order model, except γ, are independent of ϵ. As to γ, it can be assumed directly proportional to ϵ. The asymptotic states $|\tilde{A}_{\pm,\infty}|$ $(d|\tilde{A}_{\pm,\infty}|/ds=0)$ are then functions of ϵ. A simple calculation results in the bifurcation diagram in Fig. 4. Due to the global character of the instability, the prediction of the asymptotic states, as well as the values of their thresholds, are independent of the point chosen for the analysis. This has been verified at six different points throughout the flow and, in what follows, average values and standard deviations are given.

Below $\epsilon=0.0119\pm 0.0004$ two branches $|\tilde{A}_{+,\infty}|>0$ (limit cycle) and $|\tilde{A}_{+,\infty}|=0$ exist. In this regime (I), predictable by a third order theory, only one of the modes $\ell=\pm 1$ is nonzero and is selected by initial conditions. The limit torus dynamics analyzed above appears between the secondary bifurcations at $\epsilon\approx 0.012$ and $\epsilon=0.0309\pm 0.0001$ (regime II). At the latter value the amplitudes of both modes merge in an inverse pitchfork bifurcation. The frequencies then become equal and a new limit cycle (regime III) results. As the diagram shows, the applicability of the fifth order model is limited at the saddle node bifurcation at $\epsilon=0.040\pm 0.003$ unless higher order effects bring about a different bifurcation earlier.

The diagram illustrates well the way the jet behavior evolves between the threshold ($\epsilon=0$) and the value of ϵ in the simulation. A simulation at $\epsilon=0.0045$ evidences well the predicted regime I. Due to higher order effects the extrapolations to $\epsilon>0.023$ might be inaccurate and the predicted state III might not exist. A simulation at 0.036 still yields the regime II allowing to situate the actual threshold of regime III at $\epsilon=0.0377$. At $\epsilon=0.045$ a monoperiodic state with two perfectly balanced modes is reached after about 900 time units (compare to Fig. 1) confirming the existence of regime III. At this, already too high, value of ϵ, the state III is (very weakly) unstable due to a new Hopf bifurcation (1.56 times higher frequency) giving way, eventually, to a chaotic state via the type II intermittency [13]. In the presented case, the fifth order model loses thus its validity before the saddle node bifurcation is reached, otherwise, a type I intermittency would have been expected. The four regimes occur within an extremely narrow interval of the stability parameter ($\sim$4%). They might be difficult to evidence experimentally and might have escaped detecting by simply incrementing the instability parameter. The analysis of the fifth order weakly nonlinear model allowed to find instability parameters representative of all the predicted regimes without losses of CPU time.

The presented theory has been inspired by and validated on the numerical simulation of an axisymmetric cold jet. The theoretical framework based on the competition of two unstable modes arising as a result of a degenerate linear problem spectrum might, however, be of a more general interest.

[1] J. D. Crawford and E. Knobloch, Ann. Rev. Fluid Mech. **23**, 341 (1991).
[2] P. Hirschberg and E. Knobloch, Physica D **90**, 56 (1996).
[3] I. Nakamura, Phys. Fluids **19**, 5 (1976).
[4] R. Natarajan and A. Acrivos, J. Fluid Mech. **254**, 323 (1993).
[5] G. K. Batchelor and A. E. Gill, J. Fluid Mech. **14**, 529 (1962).
[6] P. J. Morris, J. Fluid Mech. **77**, 511 (1976).
[7] A. Michalke, Prog. Aerospace Sci. **21**, 159 (1984).
[8] I. Danaila, J. Dušek, and F. Anselmet, Phys. Fluids **9**, 3323 (1997).
[9] P. Huerre and P. A. Monkewitz, Ann. Rev. Fluid Mech. **22**, 473 (1990).
[10] P. Huerre and P. A. Monkewitz, J. Fluid Mech. **159**, 151 (1985).
[11] J. Dušek, P. Le Gal, and Ph. Fraunie, J. Fluid Mech. **264**, 59 (1994).
[12] T. Herbert, J. Fluid Mech. **126**, 167 (1983).
[13] P. Bergé, Y. Pomeau, and Ch. Vidal, *L'ordre dans le Chaos* (Hermann Publisher, Paris, 1988).